

# Testing Local Lorentz Invariance with Laser Tracking of the LAGEOS II satellite

David Lucchesi,<sup>1,2,3,\*</sup> Massimo Visco,<sup>1,2</sup> Roberto Peron,<sup>1,2</sup> Giuseppe Pucacco,<sup>4,2</sup> Luciano Anselmo,<sup>3</sup> Massimo Bassan,<sup>4,2</sup> Marco Cinelli,<sup>1,2</sup> Alessandro Di Marco,<sup>1,2</sup> Marco Lucente,<sup>1,2</sup> Carmelo Magnifico,<sup>1,2</sup> Carmen Pardini,<sup>3</sup> José C. Rodriguez,<sup>5</sup> and Feliciano Sapia<sup>1,2</sup>

(SaToR-G Collaboration)

<sup>1</sup>*Istituto Nazionale di Astrofisica (INAF), Istituto di Astrofisica e Planetologia Spaziali (IAPS),  
Via del Fosso del Cavaliere, 100, 00133 Roma, Italy*

<sup>2</sup>*Istituto Nazionale di Fisica Nucleare (INFN), Sezione di Tor Vergata,  
Via della Ricerca Scientifica 1, 00133 Roma, Italy*

<sup>3</sup>*Consiglio Nazionale delle Ricerche (CNR), Istituto di Scienza e  
Tecnologie della Informazione (ISTI), via G. Moruzzi 1, 56124 Pisa, Italy*

<sup>4</sup>*Dipartimento di Fisica, Università di Tor Vergata,  
Via della Ricerca Scientifica 1, 00133 Roma, Italy*

<sup>5</sup>*Geodetic Infrastructure Network, National Geographic Institute, Madrid, Spain*

(Dated: Nov. 28, 2024)

A breakdown of Lorentz Invariance is predicted by some theories as a result of quantum physics applied to gravity or for the presence of vector/tensor fields, beside the metric tensor of General Relativity, mediating the gravitational interaction. A violation of Lorentz Invariance would manifest itself, in the gravitational sector, mainly through a non-zero value of the post-Newtonian parameter  $\alpha_1$ , that is null in General Relativity. In this paper we describe a test of Local Lorentz Invariance considering the effect of a possible preferred frame, that of the cosmic microwave background, on the orbit of the LAGEOS II satellite tracked by the Satellite Laser Ranging technique. We constrain this parameter down to the level of  $3 \times 10^{-5}$ , improving a previous limit obtained through the Lunar Laser Ranging technique.

*Introduction*— Local Lorentz Invariance (LLI) states that the outcome of any local (in space and in time) non-gravitational experiment is independent from the velocity of the freely falling apparatus in which the experiment is carried out. LLI represents a cornerstone in Einstein theory of General Relativity (GR) [1] and, in particular, it represents one of the pillars of Einstein Equivalence Principle (EEP) valid in GR and in all metric theories of gravity [2]. In GR, the only field that mediates the long-range gravitational interaction is the metric tensor  $g_{\mu\nu}$ . However, in the context of modern unification theories, other fields — scalar, vector or tensor in their essence — may come to play a role in mediating the gravitational interaction in addition to the metric tensor of Einstein's theory of gravitation. In these unification theories, the action of a (four-) vector field  $K^\mu$  or of other tensor fields  $B_{\mu\nu}$ , besides  $g_{\mu\nu}$ , is such that the distribution of matter in the universe typically selects a preferred rest frame for local gravitational physics and, consequently, implies a violation of LLI. Conversely, if only one or more scalar fields are present, besides the metric tensor  $g_{\mu\nu}$ , as in the case of tensor-multi-scalar theories of gravitation [3], no violation of Lorentz Invariance is expected. From the phenomenological point of view, and in the framework of the parameterized post-Newtonian (PPN) formalism [4–7], valid in the Weak-Field and Slow-Motion (WFSM) limit of GR, the Preferred Frame Effects (PFE) are described by the parameters  $\alpha_1$ ,  $\alpha_2$  and  $\alpha_3$ , that are all equal to zero in GR and in tensor-scalar theories of gravity. LLI and, consequently, PFE, are well tested in the

context of high-energy physics experiments [8] — see also [9] for a review of Lorentz Invariance tests in effective field theories — but are much more difficult to test in the context of gravitation. Current best limits on LLI obtained in the case of Solar System tests, i.e. in the WFSM limit of GR, were achieved [10] through Lunar Laser Ranging (LLR) [11]:  $\alpha_1 = (-7 \pm 9) \times 10^{-5}$  and  $\alpha_2 = (+1.8 \pm 2.5) \times 10^{-5}$ ; and exploiting the close alignment between the spin of the Sun and the total angular momentum of the Solar system [12]:  $|\alpha_2| \lesssim 2.4 \times 10^{-7}$ . The above limits were obtained by assuming the existence of PFE with respect to the isotropic cosmic microwave background (CMB).

In this paper, we provide a new constraint on the PPN parameter  $\alpha_1$  from the analysis of the orbital residuals of the geodetic satellite LAGEOS II over a time interval of approximately 28 years (see also [13]). LAGEOS II is a passive satellite very well tracked through the powerful Satellite Laser Ranging (SLR) technique [14, 15]. In particular, we consider the possible existence of PFE due to the motion of the Earth-Sun-satellite system with respect to the CMB radiation and analyze the effect on the time evolution of a combination of Keplerian orbital parameters. This is, to our knowledge, the first measurement that constrains the PPN parameter  $\alpha_1$  using the orbit of an Earth satellite.

*Orbital effects of PFE*— In 1994, it was shown that the orbits of some artificial satellites have the potential to improve the upper limit on the  $\alpha_1$  parameter — down to the  $\sim 10^{-6}$  level — thanks to the appearance

of small divisors which enhance the corresponding PFE [16]. This possibility of reaching a stringent constraint in the PPN parameter linked to the existence of possible PFE is mainly due to the precision of the SLR tracking technique, that allows to reconstruct the orbit of a few geodetic satellites at cm level. This is the case for the two LAGEOS satellites [17–19]. For these reasons their orbital reconstruction has been exploited for fundamental physics measurements for over three decades [20–30] [31].

Starting from the Lagrangian  $\mathcal{L}$  of  $\mathcal{N}$  ideal proof-masses gravitationally interacting, it can be shown that the dependency of  $\mathcal{L}$  from the two PPN parameters  $\alpha_1$  and  $\alpha_2$  (if different from zero) will provide non-boost invariant terms depending on the velocities  $\mathbf{v}_a^0$  of the proof masses with respect to some gravitationally preferred rest frame [16]. The main effects produced if  $\alpha_1 \neq 0$  are on the eccentricity vector  $\mathbf{e}$  of the satellite's orbit [32] and on its mean argument of latitude  $\ell_0 = \omega + M$ , with  $\omega$  the argument of pericenter and  $M$  the mean anomaly of the satellite. From now on we will refer to  $\ell_0$  simply as the longitude of the satellite or observable. The first is a secular effect which is described by the sum of multiple (and independent) rotations and enhanced by small divisors in the case of particular values of the satellite's inclination. The second is a periodic effect with annual periodicity. In the present work we focus on the possible effects of the PPN  $\alpha_1$  parameter on the longitude of an artificial satellite.

Eq. (1) provides the explicit expression for a term  $\mathcal{L}_{\alpha_1}$  depending on the  $\alpha_1$  parameter in the Lagrangian when the two interacting masses are the Earth and the satellite [16]:

$$\mathcal{L}_{\alpha_1} = -\frac{\alpha_1}{2c^2} \frac{G_N m_{\oplus} m_s}{r_{\oplus s}} (\mathbf{v}_{\oplus} + \mathbf{w}) \cdot (\mathbf{v}_S + \mathbf{v}_{\oplus} + \mathbf{w}), \quad (1)$$

where  $m_{\oplus}$  and  $m_s$  are the mass of the Earth and the mass of the satellite, while  $G_N$ ,  $c$  and  $r_{\oplus s}$  are, respectively, the Newtonian Gravitational constant, the speed of light and the distances between the two masses. In Eq. (1)  $\mathbf{v}_{\oplus}$  is the velocity of the Earth with respect to the Sun,  $\mathbf{w}$  is the “absolute” (i.e. with respect to the preferred frame) velocity of the Sun, and  $\mathbf{v}_S$  is the orbital velocity of the satellite around the Earth. So,  $\mathbf{v}_{\oplus} + \mathbf{w}$  represents the “absolute” velocity of the Earth while  $\mathbf{v}_S + \mathbf{v}_{\oplus} + \mathbf{w}$  represents the “absolute” velocity of the satellite. The following two equations are the Lagrange's perturbation equations in the argument of pericenter and in the mean anomaly:

$$\frac{d\omega}{dt} = -\frac{\cos i}{na^2(1-e^2)^{1/2} \sin i} \frac{\partial \mathcal{R}}{\partial i} + \frac{(1-e^2)^{1/2}}{na^2 e} \frac{\partial \mathcal{R}}{\partial e}, \quad (2)$$

$$\frac{dM}{dt} = n - \frac{1-e^2}{na^2 e} \frac{\partial \mathcal{R}}{\partial e} - \frac{2}{na} \frac{\partial \mathcal{R}}{\partial a}, \quad (3)$$

where  $\mathcal{R}$  is the disturbing function, which is obtained from the perturbing potential of the Lagrangian [33].

If we now add up the two rates to construct the observable  $\dot{\ell}_0 = \dot{\omega} + \dot{M}$ , the terms linked to  $\partial \mathcal{R} / \partial e$  tend to cancel out, and this is truer the smaller the eccentricity of the orbit. The advantage of considering the sum of the two observables of Eqs. (2) and (3), is that most of the perturbative effects of the main gravitational and non-gravitational perturbations tend to be reduced on the final observable  $\dot{\ell}_0$  [34] By working out the dot product of Eq. (1), the disturbing function reduces to:

$$\langle \mathcal{R} \rangle_{2\pi} = -\frac{\alpha_1}{c^2} \frac{G_N m_{\oplus}}{a} (\mathbf{w} \cdot \mathbf{v}_{\oplus}), \quad (4)$$

where the notation  $\langle \mathcal{R} \rangle_{2\pi}$  implies that we take the average over the unperturbed 2-body Keplerian orbit of the satellite around the Earth. We now insert this last expression into Eqs. (2) and (3), and only retain terms that contain  $\frac{\partial \mathcal{R}}{\partial a}$  that are relevant for the effect we seek. Using Kepler third law we finally obtain:

$$\langle \dot{\ell}_0 \rangle_{2\pi} = \langle \dot{\ell}_0 \rangle_{2\pi}^{per} - 2\alpha_1 n \frac{(\mathbf{w} \cdot \mathbf{v}_{\oplus})}{c^2} + \mathcal{O}(e\alpha_1), \quad (5)$$

where the first term takes into account possible long-term periodic perturbative effects of both gravitational and non-gravitational nature. These are discussed in [13], where the main systematic errors that can affect the measurement are analyzed. To compute the term related to the PPN parameter  $\alpha_1$  we introduce the plane of the ecliptic as astronomical reference frame with the Sun at the origin, the direction  $\hat{\mathbf{x}}$  toward the Vernal Equinox  $\Upsilon$  and the  $\hat{\mathbf{z}}$  normal to the ecliptic plane. We can now compute the dot product in Eq. (5) between the two velocities that, in this frame, take the form (see Table I):

$$\mathbf{w} = w (\cos \beta_{PF} \cos \lambda_{PF} \hat{\mathbf{x}} + \cos \beta_{PF} \sin \lambda_{PF} \hat{\mathbf{y}} + \sin \beta_{PF} \hat{\mathbf{z}}), \quad (6)$$

$$\mathbf{v}_{\oplus} = v_{\oplus} (\sin(\lambda_0 + \dot{\lambda}_{\oplus} t) \hat{\mathbf{x}} - \cos(\lambda_0 + \dot{\lambda}_{\oplus} t) \hat{\mathbf{y}}). \quad (7)$$

TABLE I. Solar-system velocity  $\mathbf{w}$  with respect to the cosmic microwave background. Coordinates are in the ecliptic reference frame. The estimated errors are  $\pm 2$  km/s and  $\pm 0^\circ.01$ . Adapted from [2].

	Velocity vector $\mathbf{w}$
Absolute value: $w$	368 km/s
Latitude: $\beta_{PF}$	$-11^\circ.13$
Longitude: $\lambda_{PF}$	$171^\circ.55$

In Eq. (6), the coordinates  $(\beta_{PF}, \lambda_{PF})$  represent, respectively, the ecliptic latitude and longitude that identify the direction of the possible preferred frame represented by the CMB radiation.

In Eq. (7),  $\lambda_0$  represents the ecliptic longitude of the Earth around the Sun at a fixed epoch, while  $\dot{\lambda}_\oplus$  represents its angular orbital rate. This angular rate can be approximated with the Earth's mean motion  $n_\oplus = \sqrt{G_N M_\odot / a_{\odot\oplus}^3}$ , assuming for simplicity a circular Earth orbit (where  $M_\odot$  and  $a_{\odot\oplus}$  represent, respectively, the mass of the Sun and the astronomical unit).

Substituting these expressions for the velocities  $\mathbf{w}$  and  $\mathbf{v}_\oplus$  into Eq. (5), we finally obtain:

$$\langle \dot{\ell}_0(\alpha_1) \rangle_{2\pi} = -2\alpha_1 n \frac{wv_\oplus}{c^2} \cos \beta_{PF} \sin(\lambda_0 + n_\oplus t - \lambda_{PF}) + \dots, \quad (8)$$

where the dots represent minor contributions and we have temporarily removed the unmodeled or poorly modeled periodic effects [35].

*Orbit Determination and Residuals.* The Precise Orbit Determination (POD) of LAGEOS II has been made using GEODYN II [36] for the data reduction of the satellite normal points (NPs). The orbit analysis covers a timespan of about 28.3 years, starting from 31 October 1992 (i.e. MJD 48925). The details of the POD are described in [13]. Figure 1 shows the results for the residuals in our observable  $\dot{\ell}_0 = \dot{\omega} + \dot{M}$ , introduced to set bounds on the  $\alpha_1$  parameter [37].

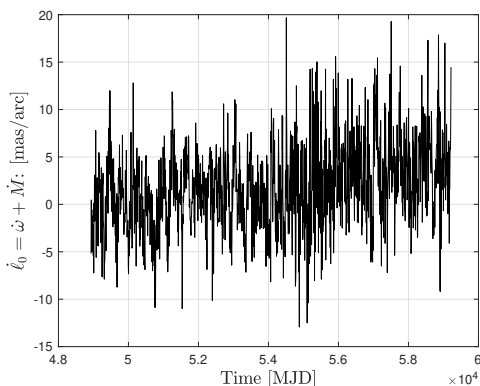


FIG. 1. LAGEOS II 7-day residuals in the rate of the longitude  $\dot{\ell}_0 = \dot{\omega} + \dot{M}$  versus time. The length of the arc is 7 days.

These residuals represent the variation of the orbital longitude over 7 days: this is the duration of an “arc”, and is the time unit of these measurements and of our analysis. The residuals contain the impact of unmodeled perturbing effects on the satellite’s orbit [38]. The presence of the possible PFE on these residuals is however masked by a plethora of gravitational and non-gravitational effects of both a periodic and secular nature. This is also clear in Figure 2 that represents the frequency domain representation, via the Fast Fourier Transform (FFT), of the residuals of Figure 1.

We are interested in detecting a signal, related to our

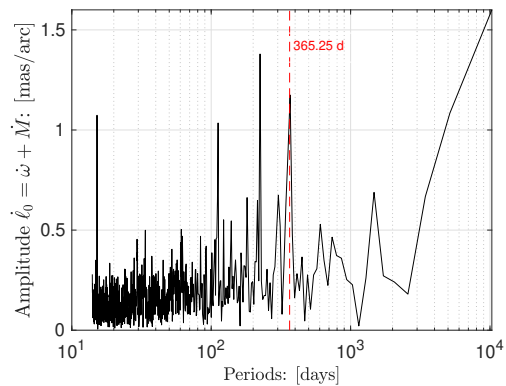


FIG. 2. FFT of the residuals in the rate of the longitude  $\dot{\ell}_0 = \dot{\omega} + \dot{M}$  of LAGEOS II over the timespan of the analysis. For ease of consultation, the plot is reversed, carrying in abscissa the periods, i.e. 1/frequency. A peak at annual periodicity is clearly visible. The sampling rate is equal to the length of the arc, i.e. 7 days.

observable, that varies with annual period and with a well defined phase. To isolate this signal from the other frequency components (see Figure 2), we adopt a Phase-Sensitive Detection (PSD) scheme: a homodyne demodulation at the target frequency (the annual one) and phase, followed by a low-pass filter [39]. In this way we obtain the amplitude of the target signal as a function of time at zero frequency. In conclusion, applying the phase-sensitive detection to Eq. (8), we finally obtain:

$$\sin(\lambda_0 + n_\oplus t - \lambda_{PF}) \langle \dot{\ell}_0(\alpha_1) \rangle_{2\pi} \simeq -\alpha_1 n \frac{wv_\oplus}{c^2} \cos \beta_{PF}. \quad (9)$$

This DC component represents the possible violation signal to be extracted from the final data.

*Measurement and Constraint*— The PSD technique was then applied to the observable of Eq. (8) according to Eq. (9) using a reference signal with annual frequency  $f_0 \simeq 2.738 \times 10^{-3} \text{ days}^{-1}$  and phase  $\phi_0 = \lambda_0 - \lambda_{PF}$ . This phase was estimated by setting the Earth’s ecliptic longitude  $\lambda_0 \simeq 223^\circ.83$  at the start date of our analysis.

Figure 3 shows the results of the in-phase component of  $\alpha_1$ . The DC component estimated from this plot represents the value of  $\alpha_1$  and, therefore, of a possible violation of the LLI:  $\alpha_1 = 2 \langle \dot{\ell}_0^{PSD} \rangle / (-2n \frac{wv_\oplus}{c^2} \cos \beta_{PF})$ , where  $\dot{\ell}_0^{PSD}$  represents our observable after the application of the PSD technique, i.e. the second member of Eq. (9).

Figure 3 also shows the PSD response (dashed line) to a modified signal obtained by reducing — through a notch filter — by a factor of 1000 the amplitude of the components having frequency within  $0.25 \text{ day}^{-1}$  around the annual frequency  $f_0$ , thus eliminating from our output every component oscillating at the sought signal frequency. As can be seen, the modified signal maintains, after the PSD, the same time behavior of the original sig-

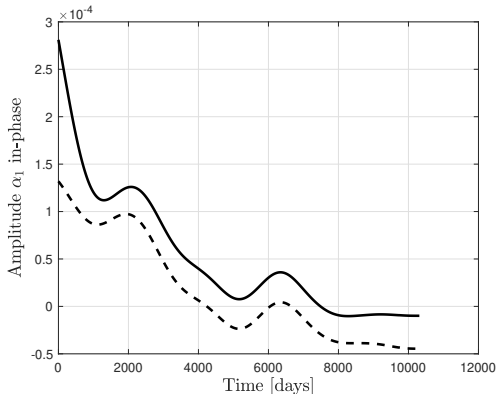


FIG. 3. Time behavior of  $\alpha_1$  after the PSD for the in-phase analysis. In this specific case we used a 3-order low-pass filter, corresponding to an attenuation of about 60 dB per decade of the amplitude of the signal above the cutoff frequency. The low-pass filter removes the higher frequencies and leaves the long-term trend we are looking for. A value of 3000 days was assumed for the integration time of the low-pass filter. The dashed lines give the PSD response to a modified signal from which the part of the signal around the annual periodicity has been significantly reduced.

nal. This suggests that the amplitude change at the PSD output is not mainly due to the behavior of the annual component.

From the PSD output in the time interval between day 2000 (MJD 50925) and day 9000 (MJD 57925), within which we do not expect a signal altered by the low-pass filter (in order to avoid ringing effects), we compute the mean and standard deviation of the constrained parameter:

$$\alpha_1 = (3 \pm 3) \times 10^{-5}. \quad (10)$$

This result is therefore compatible with a null value for the PPN parameter [40].

Figure 4 represents the estimate obtained for the parameter  $\alpha_1$  by further varying the phase of the (ideal) demodulation sinusoid: with  $\phi = [0, 2\pi]$  while keeping the reference period at 365.25 days. The black solid line shows how the estimate of the PPN parameter varies in the case of the in-phase analysis while the dashed line shows the variation of the standard deviation over the same 7000 days time interval.

The value of  $\alpha_1$  at the phase  $\phi = \phi_0 \simeq 0.91$  rad (black circle) corresponds to the specific case of Figure 3. It is worth emphasizing that the maximum value of  $\alpha_1$  is not obtained at the phase  $\phi = \phi_0$ , but at a higher value equal to approximately 2.18 rad. This reinforces our conclusion that what we obtain at the expected frequency and phase value for the violation, actually represents a null measurement for the PPN parameter.

We know of a number of perturbative effects with annual periodicity are present in the residuals of Figure 1.

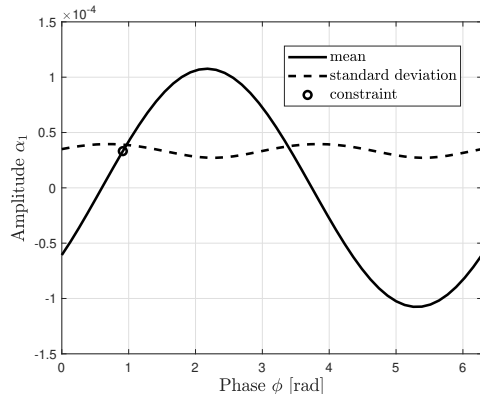


FIG. 4. Behavior of  $\alpha_1$  (black continuous line) as the phase of the demodulation sinusoid varies. The frequency of the sinusoid is fixed at the annual value. The dashed line represents the corresponding values for the standard deviation. The filter parameters are the same as those used in Figure 3.

We have therefore estimated the phase of the solid and ocean tides and the phase related to the coefficient of the quadrupole moment of the Earth's gravitational field [13]. The latter, like the tides, is characterized by a periodic oscillation (superimposed on a secular trend) with a primary component with annual periodicity, and is responsible for the largest systematic error in the measurement of the longitude of the LAGEOS II satellite. For the phase expected for the possible violation, the contribution of the main systematic errors of gravitational origin is about  $1.5 \times 10^{-5}$ .

So even the analysis of the systematic errors, although it does not fully explain the residuals which have an annual periodicity, leads us overall to the conclusion of a measurement consistent with zero for  $\alpha_1$ .

*Conclusions*— LLI represents one of the cornerstones of both the standard model of field and particle physics and the standard model of gravitation, i.e. GR. In a sense, LLI represents our current deepest understanding of the nature of space and time. So, why test LLI? A strong motivation in our work is to search for the possible evidence of *new physics* beyond GR. We mentioned the possible existence of additional fields that come into play in mediating the gravitational interaction and that could couple to matter in such a way that, in some cases, they violate Lorentz Invariance. In this work we have presented and discussed a test of LLI in the gravitational sector by searching the possible existence of PFE.

We obtained a new constraint on the PPN parameter  $\alpha_1$  from the analysis of the orbit of the geodetic satellite LAGEOS II. The result achieved is  $\alpha_1 = (3 \pm 3) \times 10^{-5}$ . The analysis has been performed on a time interval of approximately 28.3 years of the satellite orbit exploiting the precise measurements provided by the SLR technique and the main models of the GEODYN II orbit determination program.

This measurement is obtained exploiting a phase sensitive detection of the rate of the orbital residuals of LAGEOS II argument of pericenter and mean anomaly. The estimation of the main sources of systematic errors is dominated by the uncertainty on the Earth's gravitational field quadrupole coefficient  $\bar{C}_{2,0}$ , about  $2 \times 10^{-5}$  and of the same order of magnitude of the standard deviation estimated from the PSD analysis. We highlighted how the measured value for  $\alpha_1$  can correlate with the contribution of systematic errors of a gravitational nature when the contribution of the phase that we estimated for these effects at the annual frequency is introduced into the PSD analysis. The result is therefore compatible with a null value for the parameter  $\alpha_1$ , in agreement with the prediction of GR.

This is the first measurement that constraints the PPN parameter  $\alpha_1$  from the satellite orbital data in the terrestrial field. The measurement improves the previous constraint for  $\alpha_1$  obtained by means of the LLR technique [10] in the field of the Sun by a factor of 3. The result we have obtained further constrains the possible existence of a preferred frame for local gravitational physics and, consequently, that of theories of gravitation described, in addition to the metric tensor of GR, by the presence of additional fields of tensor and/or vector nature, such as for example the case of Einstein-aether theory [41], i.e. of vector-tensor theories of gravitation [42].

*Acknowledgments*— This work has been performed by the SaToR-G (Satellite Test of Relativistic Gravity) collaboration funded by the Commissione Scientifica Nazionale (CSN2) of the Istituto Nazionale di Fisica Nucleare (INFN), to which we are very grateful. The authors acknowledge the ILRS for providing high-quality laser ranging data of the LAGEOS II satellite. This work is partially supported by ICSC – Centro Nazionale di Ricerca in High Performance Computing, Big Data and Quantum Computing, funded by European Union – NextGenerationEU.

---

\* david.lucchesi@inaf.it

- [1] A. Einstein, Die Grundlage der allgemeinen Relativitätstheorie, *Annalen der Physik* **354**, 769 (1916).
- [2] C. M. Will, *Theory and Experiment in Gravitational Physics* (Cambridge University Press, Cambridge, UK, 2018).
- [3] T. Damour and G. Esposito-Farese, Tensor-multi-scalar theories of gravitation, *Classical and Quantum Gravity* **9**, 2093 (1992).
- [4] K. Nordtvedt, Equivalence Principle for Massive Bodies. II. Theory, *Phys. Rev.* **169**, 1017 (1968).
- [5] C. M. Will, Theoretical Frameworks for Testing Relativistic Gravity. II. Parametrized Post-Newtonian Hydrodynamics, and the Nordtvedt Effect, *Astrophys. J.* **163**, 611 (1971).
- [6] J. K. Nordtvedt and C. M. Will, Conservation Laws and Preferred Frames in Relativistic Gravity. II. Experimental Evidence to Rule Out Preferred-Frame Theories of Gravity, *Astrophys. J.* **177**, 775 (1972).
- [7] C. M. Will and J. K. Nordtvedt, Conservation Laws and Preferred Frames in Relativistic Gravity. I. Preferred-Frame Theories and an Extended PPN Formalism, *Astrophys. J.* **177**, 757 (1972).
- [8] D. Mattingly, Modern Tests of Lorentz Invariance, *Living Reviews in Relativity* **8**, 5 (2005), arXiv:gr-qc/0502097 [gr-qc].
- [9] S. Liberati, Tests of Lorentz invariance: a 2013 update, *Classical and Quantum Gravity* **30**, 133001 (2013), arXiv:1304.5795 [gr-qc].
- [10] J. Müller, J. G. Williams, and S. G. Turyshev, Lunar Laser Ranging Contributions to Relativity and Geodesy, in *Lasers, Clocks and Drag-Free Control: Exploration of Relativistic Gravity in Space*, edited by H. Dittus, C. Lammerzahl, & S. G. Turyshev (2008) pp. 457–472.
- [11] P. L. Bender, D. G. Currie, R. H. Dicke, D. H. Eckhardt, J. E. Faller, W. M. Kaula, J. D. Mulholland, H. H. Plotkin, S. K. Poultney, E. C. Silverberg, D. T. Wilkinson, J. G. Williams, and C. O. Alley, The Lunar Laser Ranging Experiment, *Science* **182**, 229 (1973).
- [12] K. Nordtvedt, Probing Gravity to the Second Post-Newtonian Order and to One Part in  $10^7$  Using the Spin Axis of the Sun, *Astrophys. J.* **320**, 871 (1987).
- [13] D. M. Lucchesi and et al., A Local Lorentz Invariance test with LAGEOS II satellite, *Phys. Rev. D* (2024).
- [14] M. R. Pearlman, J. J. Degnan, and J. M. Bosworth, The International Laser Ranging Service, *Adv. Space Res.* **30**, 135 (2002).
- [15] M. R. Pearlman, C. E. Noll, E. C. Pavlis, F. G. Lemoine, L. Combrink, J. J. Degnan, G. Kirchner, and U. Schreiber, The ILRS: approaching 20 years and planning for the future, *Journal of Geodesy* **93**, 2161 (2019).
- [16] T. Damour and G. Esposito-Farèse, Testing for preferred-frame effects in gravity with artificial Earth satellites, *Phys. Rev. D* **49**, 1693 (1994), gr-qc/9311034.
- [17] C. W. Johnson, C. A. Lundquist, and J. L. Zurasky, eds., *Anaheim International Astronautical Federation Congress* (1976).
- [18] NASA, *LAGEOS Phase B Technical Report, NASA Technical Memorandum X-64915*, Tech. Rep. TMX-64915 (Marshall Space Flight Center, Marshall Space Flight Center, Alabama 35812, 1975) february 1975.
- [19] F. Fontana, *Physical properties of LAGEOS II satellite*, Tech. Rep. LG-TN-AI-037 (Aeritalia, 1989).
- [20] I. Ciufolini, D. Lucchesi, F. Vespe, and A. Mandiello, Measurement of dragging of inertial frames and gravitomagnetic field using laser-ranged satellites., *Nuovo Cim. A* **109**, 575 (1996).
- [21] I. Ciufolini and E. C. Pavlis, A confirmation of the general relativistic prediction of the Lense-Thirring effect, *Nature* **431**, 958 (2004).
- [22] D. M. Lucchesi, The Lense-Thirring effect derivation and the LAGEOS satellites orbit analysis with the new gravity field solution from CHAMP, in *35th COSPAR Scientific Assembly*, COSPAR Meeting, Vol. 35, edited by J.-P. Paillé (2004) p. 232.
- [23] D. M. Lucchesi and R. Peron, Accurate Measurement in the Field of the Earth of the General-Relativistic Precession of the LAGEOS II Pericenter and New Constraints on Non-Newtonian Gravity, *Phys. Rev. Lett.* **105**, 231103 (2010).

- [24] D. M. Lucchesi and R. Peron, LAGEOS II pericenter general relativistic precession (1993-2005): Error budget and constraints in gravitational physics, *Phys. Rev. D* **89**, 082002 (2014).
- [25] D. Lucchesi, L. Anselmo, M. Bassan, C. Pardini, R. Peron, G. Pucacco, and M. Visco, Testing the gravitational interaction in the field of the Earth via satellite laser ranging and the Laser Ranged Satellites Experiment (LARASE), *Class. Quantum Grav.* **32**, 155012 (2015).
- [26] D. M. Lucchesi, L. Anselmo, M. Bassan, C. Magnafico, C. Pardini, R. Peron, G. Pucacco, and M. Visco, General Relativity Measurements in the Field of Earth with Laser-Ranged Satellites: State of the Art and Perspectives, *Universe* **5**, 141 (2019).
- [27] D. M. Lucchesi, M. Visco, R. Peron, M. Bassan, G. Pucacco, C. Pardini, L. Anselmo, and C. Magnafico, An improved measurement of the Lense-Thirring precession on the orbits of laser-ranged satellites with an accuracy approaching the 1% level, arXiv e-prints, arXiv:1910.01941 (2019), arXiv:1910.01941 [gr-qc].
- [28] I. Ciufolini, A. Paolozzi, E. C. Pavlis, G. Sindoni, J. Ries, R. Matzner, R. Koenig, C. Paris, V. Gurzadyan, and R. Penrose, An improved test of the general relativistic effect of frame-dragging using the LARES and LAGEOS satellites, *European Physical Journal C* **79**, 872 (2019), arXiv:1910.09908 [gr-qc].
- [29] D. Lucchesi, M. Visco, R. Peron, M. Bassan, G. Pucacco, C. Pardini, L. Anselmo, and C. Magnafico, A 1% Measurement of the Gravitomagnetic Field of the Earth with Laser-Tracked Satellites, *Universe* **6**, 139 (2020).
- [30] D. Lucchesi, L. Anselmo, M. Bassan, M. Lucente, C. Magnafico, C. Pardini, R. Peron, G. Pucacco, and M. Visco, Testing Gravitational Theories in the Field of the Earth with the SaToR-G Experiment, *Universe* **7**, 192 (2021).
- [31] Of course, it is necessary to develop a dynamic model for the orbit of these satellites that is equally reliable and accurate [25, 26, 43, 44].
- [32] This is the Laplace-Runge-Lenz vector that identifies the satellite pericenter direction: a constant of motion in the ideal case of the 2-body Newtonian problem.
- [33] To compute the variation of the orbital elements, a linear perturbation approach is sufficient in which the right-hand side of the above perturbing equations are evaluated by keeping constant, to their (mean) nominal values, the semi-major axis  $a$ , the eccentricity  $e$ , the inclination  $i$  and the mean motion  $n = \sqrt{GM_{\oplus}/a^3}$ .
- [34] This is also true in the case of some relativistic effects, such as Schwarzschild precession [45].
- [35] These periodic effects are considered separately in the analysis of the main sources of systematic error in [13].
- [36] D. E. Pavlis and et al., *GEODYN II Operations Manual*, NASA GSFC (1998).
- [37] These residuals were obtained by adding the residuals in the rate of the argument of pericenter and in the rate of the mean anomaly of LAGEOS II, see Figure 1 in [13], after removing, on the basis of the rates reported in Table III of the same paper, the total relativistic precession predicted by GR (and not modeled in the POD) on the rate of the argument of pericenter and on the rate of the mean anomaly.
- [38] The overall period of our analysis has been divided into 7-day arcs not causally connected to each other, and the initial state-vector for each arc has been adjusted in the POD procedure to best fit the NPs.
- [39] The periodic signal that we wish to detect, after the homodyne detection, splits into a continuous component, and in a periodic component with a frequency double that of the initial one, and both components with an amplitude half of the initial one. This signal is low-pass filtered for the final analysis and measurement.
- [40] We verified that the obtained constraint did not depend on the filter characteristics, by changing its order between 3 and 5 and the integration time between 2000 and 5000 days.
- [41] T. Jacobson and D. Mattingly, Einstein-aether waves, *Phys. Rev. D* **70**, 024003 (2004).
- [42] Very interesting, the Einstein-aether theory can be seen as the low-energy limit of the Hořava-Lifshitz quantum theory [46].
- [43] M. Visco and D. M. Lucchesi, Review and critical analysis of mass and moments of inertia of the LAGEOS and LAGEOS II satellites for the LARASE program, *Advances in Space Research* **57**, 1928 (2016).
- [44] M. Visco and D. M. Lucchesi, Comprehensive model for the spin evolution of the LAGEOS and LARES satellites, *Phys. Rev. D* **98**, 044034 (2018).
- [45] M. H. Soffel and W.-B. Han, *Applied General Relativity* (2019).
- [46] P. Hořava, Spectral Dimension of the Universe in Quantum Gravity at a Lifshitz Point, *Phys. Rev. Lett.* **102**, 161301 (2009), arXiv:0902.3657 [hep-th].